Correlation and disorder effects for the electronic transport in the low-dimensional system $Na_xCa_{1-x}V_2O_5$ and $Na_xV_2O_5$

2008 J. Phys.: Condens. Matter 20 445207

(http://iopscience.iop.org/0953-8984/20/44/445207)

J. Phys.: Condens. Matter **20** (2008) 445207 (7pp) doi:10.1088/0953-8984/20/44/445207

Correlation and disorder effects for the electronic transport in the low-dimensional system $Na_xCa_{1-x}V_2O_5$ and $Na_xV_2O_5$

Masashige Onoda and Yoshikazu Mizuguchi

Institute of Physics, University of Tsukuba, Tennodai, Tsukuba 305-8571, Japan

E-mail: onoda@sakura.cc.tsukuba.ac.jp

Received 16 June 2008, in final form 5 September 2008
Published 30 September 2008
Online at stacks.iop.org/JPhysCM/20/445207

Abstract

The transport properties of extra carriers introduced in the Mott insulator NaV_2O_5 with coupled V–O–V molecular orbitals have been explored through measurements of the x-ray powder diffraction, electrical resistivities and thermoelectric powers for $Na_xCa_{1-x}V_2O_5$ with $0.83 \leqslant x < 1$ and $Na_xV_2O_5$ with $0.8 \leqslant x < 1$. These systems have electron and hole carriers for $x < 1$, respectively. In the vicinity of the average V valence of 4.5, the Mott-type one-dimensional variable-range hopping mechanism for coupled chains may be effective, and a linear relation between the hopping energy and the thermoelectric power is found. The composition dependences of thermoelectric powers are almost understood in terms of the Heikes formula in a strongly correlated region with the number of electrons per coupled orbital. The effects of the electron correlation and the atomic disorder for the transport properties may be closely related to each other.

1. Introduction

Transition-metal oxides and ternary oxide bronzes have provided various fields of research such as correlated electron systems, quantum spin-fluctuation systems or novel function systems.

The vanadium oxide system has a variety of low-dimensional spin networks. In the half-filled insulator system, the series CaV_nO_{2n+1} ($n = 2$–4) with two-dimensional spin-$\frac{1}{2}$ networks at the V^{4+} site [1–3] has attracted much attention. For $n = 2$ and 4, spin-singlet states are formed, basically due to dimerization for the corner-sharing rung in a trellis layer [3] and to weakly coupled metaplaquettes [4], respectively. On the other hand, for $n = 3$, a stripe-phase magnetic order takes place [5]. The double trellis-layer system with a partially filled d-band has also been investigated in detail [6].

The quarter-filled compound NaV_2O_5, which has an orthorhombic structure similar to that of CaV_2O_5 [3, 7, 8] as shown in figure 1, exhibits one-dimensional spin-$\frac{1}{2}$ magnetic properties with a V–O–V molecular orbital for the rung in the trellis layer [7, 9] and undergoes a transition to the singlet state [10] with a lattice distortion and a partial valence order [11]. While the singlet transition with the partial valence order in NaV_2O_5 has been mainly investigated from various viewpoints, the transport mechanism for the quarter-filled state has been little discussed except for the insulating nature of this compound.

This work plans to explore the detailed transport properties of the extra carriers introduced in the Mott insulator NaV_2O_5 with the V–O–V molecular orbital. The transport mechanism will be discussed on the basis of results of the electrical resistivity and thermoelectric power for single-crystal and polycrystalline specimens of $Na_xCa_{1-x}V_2O_5$ and $Na_xV_2O_5$. Here, the average valences of V ions in these systems are expressed as $\alpha = 4+x/2$ and $5-x/2$, respectively, from the nominal composition. Considering that NaV_2O_5 is the quarter-filled Mott insulator, $(1-x)/2$ carriers are doped in $Na_xCa_{1-x}V_2O_5$ as an electron and in $Na_xV_2O_5$ as a hole with decreasing x from unity. The experimental methods for sample preparations and characterizations are described in section 2. The structural characteristics explored by means of

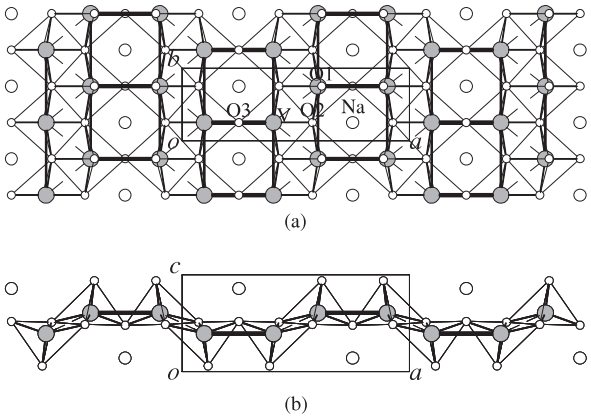

Figure 1. The crystal structure of NaV_2O_5 projected onto (a) the *ab*- and (b) *ac*-planes after [7, 8], where the thin lines indicate the edges of VO_5 pyramids. The broken lines and the thick lines denote the edge-sharing V–V path and the corner-sharing ones, respectively.

the x-ray powder diffraction are discussed in section 3.1, and the transport properties based on the electrical resistivity and thermoelectric power are in sections 3.2 and 3.3, respectively. Section 4 is devoted to conclusions.

2. Experiments

Polycrystalline specimens of $Na_xCa_{1-x}V_2O_5$ with nominal compositions of $0.85 \leqslant x \leqslant 1$ were prepared by solid-state reaction methods, heating sealed mixtures of $x NaVO_3$, $(1-x)CaVO_3$ and VO_2 at temperatures from 958 ($x = 1$) to 1008 K ($x = 0.85$) depending on x, and those of $Na_xV_2O_5$ with $0.72 \leqslant x \leqslant 1$ were made from $x NaVO_3$, $(1-\frac{3x}{4})V_2O_5$ and $\frac{x}{4}V_2O_3$ at 958 K. Here, $NaVO_3$ and VO_2 were obtained following the procedure described in [8], and $CaVO_3$ and V_2O_3 as in [12]. The single crystals of NaV_2O_5 and $Na_{0.83}Ca_{0.17}V_2O_5$ were the same as those in [8] and those of $Na_xV_2O_5$ with $x \neq 1$ were obtained by annealing NaV_2O_5 crystals covered with the non-stoichiometric powders. No chemical analysis was done.

An x-ray powder diffraction pattern was taken with Cu Kα radiation at 293 K using a Rigaku RAD-IIC diffractometer. The four-terminal electrical resistivity and the thermoelectric power were measured with a dc method at temperatures mostly in the range from 80 to 300 K, this range being limited by the resistivity of the specimen at low temperatures (about 10^6 Ω cm at maximum) and prevention of possible deterioration of the specimen at high temperatures. Here, the resistivity along the *c*-axis corresponding to the direction normal to the growing *ab*-plane of the single crystals was measured by making current and voltage terminals with a silver paste on each plane, while those along the *a*- and *b*-axes were done with a standard contact. For the thermoelectric voltage, gold electrodes were used and the contacts were made with a gold paste; and then the absolute thermoelectric powers were obtained by use of the calibrated absolute thermoelectric powers of gold.

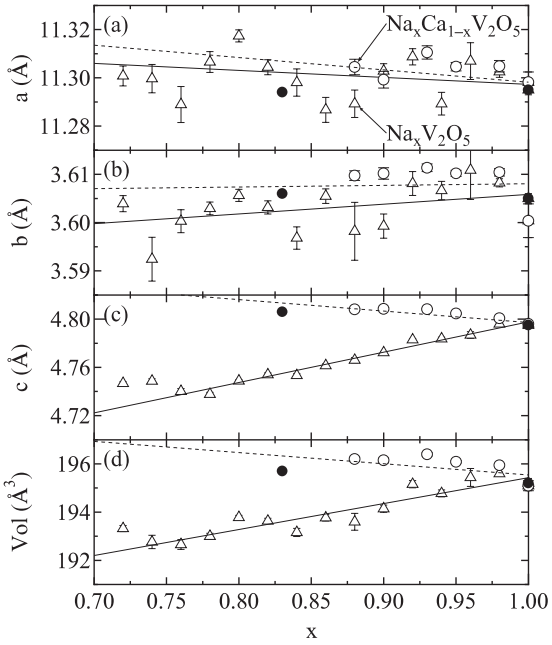

Figure 2. The composition dependences of lattice constants for $Na_xCa_{1-x}V_2O_5$ and $Na_xV_2O_5$ at 293 K, where the dotted and full lines indicate fits based on the Vegard law, the former being drawn including the data of CaV_2O_5 [3]. The full symbols show the results based on the x-ray four-circle diffraction [8].

3. Results and discussions

3.1. Structural properties

The polycrystalline specimens of $Na_xCa_{1-x}V_2O_5$ with $0.9 \leqslant x \leqslant 1$ and $Na_xV_2O_5$ with $0.8 \leqslant x \leqslant 1$ are a single phase having powder diffraction patterns similar to those calculated on the basis of the atomic parameters determined from the single-crystal diffraction of NaV_2O_5 [8]. Figure 2 shows the composition dependences of the lattice constants at 293 K. Here, the dotted lines for $Na_xCa_{1-x}V_2O_5$ and the full lines for $Na_xV_2O_5$ indicate fits according to the Vegard law, the former being drawn including the data for CaV_2O_5 [3]. For both of the systems, the constants a and b do not vary significantly with x, whereas c, the distance between the trellis layers, (see figure 1(b)) changes. The increase of the volume for $Na_xCa_{1-x}V_2O_5$ and the decrease for $Na_xV_2O_5$ with decreasing x correspond to the continuous expansion of the volume with decreasing average V valence, which is consistent with a change of the radius of V ions having pyramidal coordinations expected from the chemical formula; that is, 0.53 Å for V^{4+} and 0.46 Å for V^{5+} [13].

3.2. Electrical resistivities

For all of the specimens measured, where the results for the compositions having a second phase are not described, the electrical resistivities ρ apparently indicate nonmetallic behaviour. For the single crystal with $x = 1$, NaV_2O_5, the resistivities ρ_s^i for $i = a$-, b- and c-axes at room temperature are $\rho_s^a \simeq 2$, $\rho_s^b \simeq 0.7$ and $\rho_s^c \simeq 30$ kΩ cm, respectively, and their ratio is 3:1:40, indicating that the electronic states of this

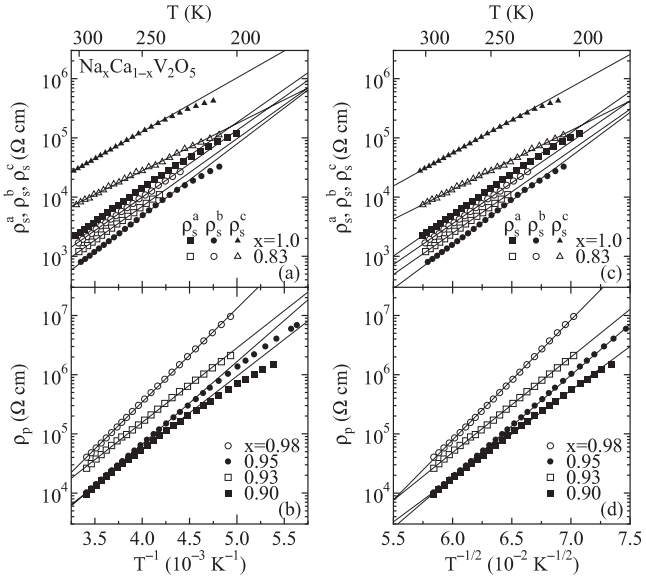

Figure 3. The electrical resistivities of (a) the single-crystal and (b) polycrystalline specimens for $Na_xCa_{1-x}V_2O_5$ as a function of T^{-1}; and ((c), (d)) those against $T^{-1/2}$. Here, the full lines in ((a), (b)) and ((c), (d)) are fits to equations (1) and (2) with $d = 1$, respectively, with parameters plotted in figure 4.

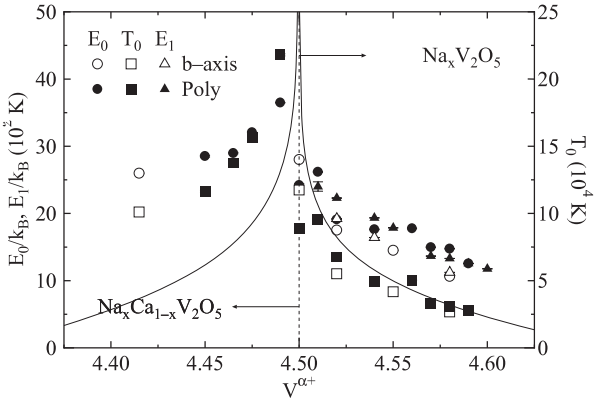

Figure 4. The average V valence dependences of the characteristic energies E_0, T_0 and E_1 determined from the fits to equations (1), (2) with $d = 1$ and (6), respectively, for $Na_xCa_{1-x}V_2O_5$ and $Na_xV_2O_5$. Here, the full curves represent T_0 deduced from equations (4) and (7).

composition may be one-dimensional for the b-axis as pointed out previously [14]. For the single crystal of $Na_{0.83}Ca_{0.17}V_2O_5$, $\rho_s^a \simeq 1$, $\rho_s^b \simeq 1$ and $\rho_s^c \simeq 7\,k\Omega$ cm, which suggests an increase of the dimensionality for conduction. Therefore, a crossover between one- and two-dimensional conduction may take place at a certain composition in $Na_xCa_{1-x}V_2O_5$, but it is out of the scope of our paper.

In the following, let us use the thermally activated model and the variable-range hopping (VRH) model, which are often applied to data at high and low temperatures, respectively. At intermediate temperatures, there is a contribution from both these transports at the same time. First, let us see how the activation model and the VRH model explain the data. The resistivities as a function of T^{-1} for single crystals of $Na_xCa_{1-x}V_2O_5$ are shown in figure 3(a). On the high-temperature side, they follow the thermally activated formula of

$$\rho_A \propto \exp\left[E_0/(k_B T)\right], \tag{1}$$

where E_0 and k_B are the activation energy and Boltzmann constant, respectively, as shown by the full lines. Here, for the a-, b- and c-axes of NaV_2O_5, $E_0/k_B = 2.6$, 2.8 and 2.1×10^3 K, respectively. This distribution of E_0 may be mainly attributed to sample dependences, since the measurements have been performed for different crystals owing to the small size of platelets. In addition, ρ_s^c is expected to have slight contributions from ρ_s^a and ρ_s^b owing to the difficulty in making precise contacts in this direction normal to the growing plane. That is, the relatively small E_0 value for the c-axis is imprecise, but it is considered to be meaningful to indicate that E_0 for ρ_s^c is not so different from those for ρ_s^a and ρ_s^b. Thus, E_0/k_B may be $2.5(3) \times 10^3$ K on average and it does not have a significant anisotropy. The band gap defined as twice E_0 is close to the correlated band gap derived in the framework of the Hubbard-like model [15] with the assumption of small bandwidth. $Na_{0.83}Ca_{0.17}V_2O_5$ also has a similar band gap as plotted against the average V valence α calculated from the chemical formula in figure 4. Figure 3(b) indicates the resistivities ρ_p against T^{-1} for the polycrystalline specimens of $Na_xCa_{1-x}V_2O_5$. The resistivities at room temperature that have a rough tendency to decrease with decreasing x are one order of magnitude larger than those for the b-axis with a similar composition, which implies that a parallel combination model of the resistivity is not always applicable to the present data, since it would predominantly reflect the resistivity for the b-axis. The full lines based on equation (1) give the α dependences of E_0 shown in figure 4.

For the VRH model given as

$$\rho_V \propto \exp(T_0/T)^{1/(1+d)}, \tag{2}$$

where d is 1, 2 or 3, the value of $d = 1$ explains the temperature dependences of ρ_p well. On the other hand, for single crystals of NaV_2O_5 and $Na_{0.83}Ca_{0.17}V_2O_5$, it is difficult to judge whether the VRH model is effective or not from the present data alone, since the temperature ranges measured are rather limited. ρ_s^i and ρ_p as a function of $T^{-1/2}$ for $Na_xCa_{1-x}V_2O_5$ are shown in figures 3(c) and (d), respectively. The α dependences of T_0 estimated from the full lines are plotted in figure 4. These considerations of resistivity data for $Na_xCa_{1-x}V_2O_5$ suggest that the transport phenomena for $x = 1$ and $0.83 < x < 1$ follow equations (1) and (2) with $d = 1$, respectively.

The temperature dependences of resistivities ρ_s^b and ρ_p of the single-crystal b-axis and polycrystalline specimens for $Na_xV_2O_5$ are shown in figures 5(a) and (b), respectively, and those against $T^{-1/2}$ are in figures 5(c) and (d). The resistivities at room temperature are reduced significantly with decreasing x as in the case of $Na_xCa_{1-x}V_2O_5$. The VRH model in equation (2) with $d = 1$ explains the data for $\alpha > 4.5$ over the wide range of temperatures, and it is more appropriate than the activation model in equation (1). The average V valence dependences for E_0 and T_0 estimated from the full lines in

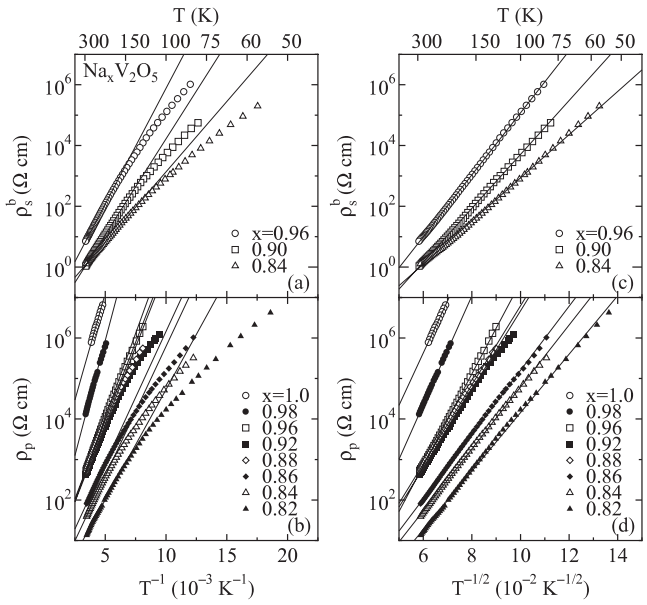

Figure 5. The electrical resistivities of (a) the single-crystal *b*-axis and (b) polycrystalline specimens for $Na_xV_2O_5$ as a function of T^{-1}; and ((c), (d)) those against $T^{-1/2}$. Here, the full lines in ((a), (b)) and ((c), (d)) are fits to equations (1) and (2) with $d = 1$, respectively, with parameters plotted in figure 4.

figures 5((a), (b)) and ((c), (d)), respectively, are provided in figure 4. The E_0 and T_0 values estimated on the single-crystal data agree roughly with those for the polycrystalline ones; in other words, the values for the polycrystalline specimens of $Na_xV_2O_5$ may be intrinsic and they do not have a significant anisotropy, consistent with the single-crystal results for NaV_2O_5 and $Na_{0.83}Ca_{0.17}V_2O_5$ mentioned above.

The hopping exponent of $d = 1$ in equation (2) suggests that the transport mechanism is either Efros–Shklovskii (ES) type in two and three dimensions [16–18] or Mott type in one dimension [18–20]. The former is based on a soft gap Δ due to long-range Coulomb interactions between the localized electrons, and the latter type is for the conduction of one electron through intermediately localized orbitals in a random potential, which also appears in weakly coupled chains [21] or finite chains [22, 23]. On the basis of the ES-type VRH in two dimensions, T_0 in equation (2) is expressed by $T_0 = 6.2e^2/(k_B K\xi)$, where e, K and ξ are the absolute values of the electron charge, the dielectric constant of the medium and the localization length, respectively [16–18]. Taking the K value of about 30 [24] for $T_0 \approx 10^5$ K, ξ is estimated to be about 0.3 Å, which may be rather small. The upper limit of temperature where the ES mechanism is appropriate is evaluated as $T_{ES} = 6.2\Delta^2/(k_B^2 T_0)$. The condition of $T_{ES} \geqslant 3 \times 10^2$ K leads to $\Delta/k_B \geqslant 2 \times 10^3$ K. Then, the density of states defined as $D = \Delta K^2/(e^4\pi)$ is estimated to be larger than 3×10^{15} eV^{-1} cm^{-2}, which is significantly larger than the value for this system. The case in three dimension also provides anomalously large D. Therefore, the Mott-type VRH is effective in the temperature range of measurements. According to this mechanism for coupled chains, T_0 is given by $T_0 = 4/(k_B D'\xi)$, where D' is the constant density of states [18]. Here, it is noted that the intrachain VRH resistivity without any interchain coupling should provide an activation-type temperature dependence which is the same as that for a single infinite chain [25]. In addition, the VRH resistivity for coupled chains is known to lead to the weaker (three-dimensional) temperature variation at low temperatures depending on the bandwidth in the transverse direction [21].

As described before, the VRH state is preferable for the transport properties with $\alpha \neq 4.5$ in the temperature range measured. All of the compounds exhibit nonmetallic properties, which are likely attributed to the small bandwidth W due to the orbital singlet in VO_5 pyramids and that due to the atomic disorder. Let us consider the α dependence of T_0 for $Na_xCa_{1-x}V_2O_5$ and $Na_xV_2O_5$ shown in figure 4. For the region $\alpha < 4.5$ corresponding to a crossover between the Mott insulator NaV_2O_5 and the spin-gapped Mott insulator CaV_2O_5, T_0 is reduced with decreasing α. Similarly, in another crossover of $\alpha > 4.5$ between NaV_2O_5 and the band insulator V_2O_5, it is significantly reduced with increasing α. T_0 has a maximum at around $\alpha = 4.5$. The reduction of T_0 may be caused by the increase of localization length for the band with a constant density of states around the Fermi level μ. The difference of the magnitudes of T_0 above and below $\alpha = 4.5$ suggests that the detailed electronic structures for $\alpha < 4.5$ and $\alpha > 4.5$ are a little asymmetric due to the existence of the V–O–V molecular orbital. In fact, a decrease of resistivity with the Na deficiency is notable as compared with the case of Na–Ca substitution. The VRH-like insulator state due to the disorder effect is known to appear, accompanied with a significant increase of effective mass, in the perovskite Ti oxides near the metal–insulator crossover [26, 27]. Since it is not easy to prepare perfect stoichiometric transition-metal compounds, the VRH-like state sometimes appears even in the apparent Mott insulator phase.

3.3. Thermoelectric powers

The thermoelectric power S, which is not significantly influenced by the intergrain transport, should better reflect the intrinsic properties. The temperature dependences of thermoelectric powers S_s^i and S_p for the single-crystal and polycrystalline specimens of $Na_xCa_{1-x}V_2O_5$ are plotted in figures 6(a) and (b), respectively. NaV_2O_5 has nearly temperature-independent positive values in the temperature range measured precisely, indicating the carriers to be holes. As expected from the resistivity results, the anisotropy of S is significant: for the *b*-axis or the one-dimensional direction of the resistivity, $S_s^b \approx 700$ μV K^{-1} at room temperature, while for the *c*-axis or the interlayer direction, $S_s^c \approx 20$ μV K^{-1}. This may be explained considering the conductivity weighted thermoelectric power [28] expressed as

$$S_s^i = \sigma_s^i S \Big/ \sum_i \sigma_s^i, \tag{3}$$

where σ_s^i is the principal value of the conductivity tensor, corresponding to the crystallographic axis. In NaV_2O_5, the ratio of $\sigma_s^i / \sum_i \sigma_s^i$ for $i = a$, b and c at room temperature is roughly 0.35:1:0.023, close to the anisotropy of S. A slight

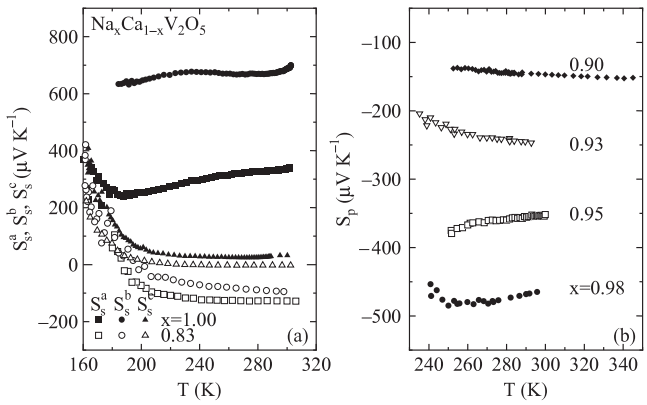

Figure 6. The temperature dependences of thermoelectric powers of (a) the single-crystal and (b) polycrystalline specimens for $Na_xCa_{1-x}V_2O_5$.

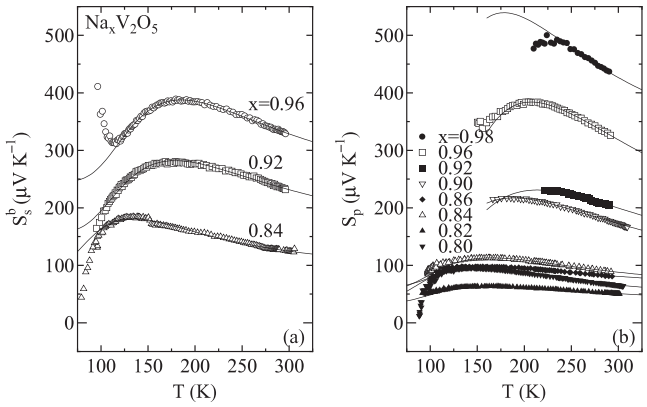

Figure 7. The temperature dependences of thermoelectric powers of (a) the single-crystal *b*-axis and (b) polycrystalline specimens for $Na_xV_2O_5$, where the full curves are fits to equation (6).

decrease of x leads to a large negative value, indicative of electron carriers: for the polycrystal with $x = 0.98$, $S_p \approx -470\ \mu V\ K^{-1}$. On decreasing x further, the absolute value of negative S decreases rapidly. For all of the compounds, the thermal variations at high temperatures are not significant. The anisotropy of S observed for $Na_{0.83}Ca_{0.17}V_2O_5$ single crystals is almost explained in terms of equation (3) with $\sigma_s^a \approx \sigma_s^b > \sigma_s^c$ as pointed out in section 3.2.

The temperature dependences of thermoelectric powers for the single-crystal *b*-axis and polycrystalline specimens of $Na_xV_2O_5$ are shown in figures 7(a) and (b), respectively. All of the data are positive as in the case of NaV_2O_5. With decreasing temperature, they increase gradually and exhibit broad maxima.

In section 3.2, the transport for $\alpha \neq 4.5$ is found to be the Mott-type VRH in one dimension. The thermoelectric power in this mechanism is written as [18, 29]

$$S_V = \frac{k_B}{2eD\xi}\left[\frac{\partial \ln D(\epsilon)}{\partial \epsilon}\right]_{\epsilon=\mu} = \frac{k_B^2 T_0}{8e}\left[\frac{\partial \ln D(\epsilon)}{\partial \epsilon}\right]_{\epsilon=\mu}, \quad (4)$$

where all of the quantities are already defined in section 3.2 and this equation should be valid for $T > T_{ES}$. Thus,

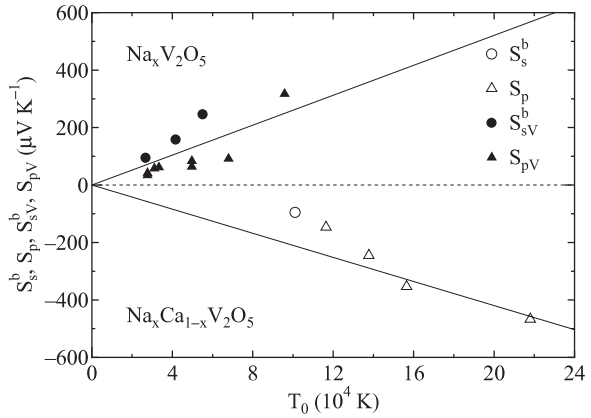

Figure 8. The thermoelectric powers against the hopping energy for $Na_xCa_{1-x}V_2O_5$ and $Na_xV_2O_5$, where the full lines show the relation of $S \propto T_0$.

S is temperature-independent and linear in T_0 for a nearly constant energy-derivative of $\ln D(\epsilon)$ against the average V valence. This property may be consistent with the results for $Na_xCa_{1-x}V_2O_5$. On the other hand, since the results for $Na_xV_2O_5$ depend on temperature even at high temperatures, it is necessary to consider the intrachain hopping with the gap E_1. The thermoelectric power for this process is expressed as

$$S_I = k_B E_1/(eT). \quad (5)$$

The thermoelectric power with the VRH and intrachain hopping processes should have the form of

$$S = (\sigma_V S_V + \sigma_A S_I)/(\sigma_V + \sigma_A), \quad (6)$$

where $\sigma_{V,A}$ are the inverse of equations (2) and (1), respectively, and E_0 is replaced with E_1. On the assumption of $\sigma_V > \sigma_A$ for T_0 determined in section 3.2, fits to equation (6) provide the values of S_{sV}^b and S_{pV} shown in figures 8 and 9, and E_1 in figure 4 from full curves drawn in figures 7(a) and (b). This model gives S_V at the high-and low-temperature limits and leads to a maximum at an intermediate temperature, which almost accounts for the data of $Na_xV_2O_5$. The α dependence of E_1 nearly agrees with that of E_0 determined at high temperatures, which should provide the gap for the intrachain. The reason why the maximum phenomena do not exist in $Na_xCa_{1-x}V_2O_5$ is that σ_V is significantly larger than σ_A.

The T_0 dependences of S_s^b and S_p for $Na_xCa_{1-x}V_2O_5$ at 300 K regarded as temperature-independent values and those of S_{sV}^b and S_{pV} for $Na_xV_2O_5$ estimated above are shown in figure 8. The relation of $S \propto T_0$ is roughly valid, as indicated by the full lines, which suggests that the VRH transport is effective for the both systems with $x \neq 1$. The absolute values of S/T_0 for $\alpha > 4.5$ and $\alpha < 4.5$ almost agree with each other. Here, the deviation from the full line for the small range of T_0 in $Na_xCa_{1-x}V_2O_5$ would be attributed to the increase of the dimensionality for conduction as suggested in section 3.2. On the basis of these results, VRH transport is concluded to be effective in the vicinity of the Mott insulator.

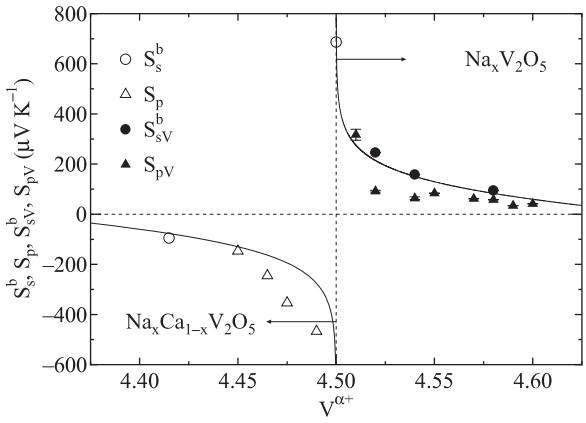

Figure 9. The thermoelectric powers as a function of the average V valence for $Na_xCa_{1-x}V_2O_5$ and $Na_xV_2O_5$, where the full curves indicate results calculated from equation (7) for the coupled V orbitals.

Figure 9 shows S^b_s and S_p for $Na_xCa_{1-x}V_2O_5$ at 300 K, and S^b_{sV} and S_{pV} for $Na_xV_2O_5$ as a function of the average V valence. The results for the electron-carrier side of $Na_xCa_{1-x}V_2O_5$ ($\alpha < 4.5$), and those for the hole-carrier side of $Na_xV_2O_5$ ($\alpha > 4.5$), are found to be roughly point symmetric at $\alpha = 4.5$. Since this result approximates to the high-temperature limit, let us use the Heikes formula

$$S_H(n) = -\frac{k_B}{e} \ln \frac{2(1-n)}{n}, \qquad (7)$$

for the case of T, $U \gg W$ but $T \ll U$, T and U being the temperature and the on-site Coulomb repulsion energy, respectively [30]. NaV_2O_5 is the quarter-filled insulator or the half-filled insulator per coupled V–O–V orbital, so that the number of effective carriers is given by $n = 2(5-\alpha)$. For $\alpha < 4.5$, $S_H(2-n) = -S_H(n)$ due to the electron–hole symmetry. As shown by the full curves in figure 9, the calculated values based on equation (7) account for the results. Here, it should be noted that the present NaV_2O_5 indicates a large positive value. This is consistent with recent theoretical considerations in the one-dimensional Hubbard model [31]. Although the thermoelectric power for the Mott insulator composition should be zero by the electron–hole symmetry in that model, phonon modulation for U is known to destroy this symmetry, giving rise to a nonzero value [32]. This effect, as well as the inevitably slight difference of the composition, may provide the present results.

The results for $Na_xCa_{1-x}V_2O_5$ and $Na_xV_2O_5$ in figures 8 and 9 indicate that both equations (4) and (7) may be valid in the vicinity of the Mott insulator, which are attributed to the effects of atomic disorder and electron correlation, respectively. Here, it should be noted that equation (4) is applied at temperatures where the VRH transport is relevant, while equation (7) is at the high-temperature limit. Combining these equations, we get the α dependence of T_0 shown by the full curves in figure 4. The reason why the system does not become metallic for $x \neq 1$ is that the bandwidth may be rather small, although it may increase with decreasing x as suggested from the E_0 behaviours shown in figure 4. For the large x in $Na_xCa_{1-x}V_2O_5$, that relation is not valid. In order to discuss the transport mechanism of this system, a crossover between the dimer state and the V–O–V orbital state, and that between the one- and two-dimensional conductions should be clarified.

4. Conclusions

The transport properties of extra carriers introduced in the Mott insulator NaV_2O_5 with coupled V–O–V molecular orbitals have been investigated through measurements of the x-ray powder diffraction, electrical resistivities and thermoelectric powers for the single-crystal and polycrystalline specimens of $Na_xCa_{1-x}V_2O_5$ and $Na_xV_2O_5$.

The $Na_xCa_{1-x}V_2O_5$ and $Na_xV_2O_5$ systems have electron and hole carriers for $0.83 \leqslant x < 1$ and $0.8 \leqslant x < 1$, respectively. The nonmetallic behaviours of electrical resistivities are considered on the basis of activation and VRH models. The correlation gap estimated for the nominal composition NaV_2O_5 is almost consistent with the theoretical result. For both of the systems, the Mott-type one-dimensional VRH mechanism for coupled chains may be effective in the temperature range measured, and a linear relation between the thermoelectric power and the VRH hopping energy is found in the vicinity of the Mott insulator. For the electron carriers with $\alpha < 4.5$, this relation becomes poor as the system approaches the composition CaV_2O_5, likely due to a complicated crossover process between the dimer state and the V–O–V orbital state, and that between the one- and two-dimensional transports. It is also found that the band gap in the intrachain for $Na_xV_2O_5$ has a tendency to decrease with decreasing x and the anisotropies of thermoelectric powers are explained with the conductivity weighted scheme. In the high-temperature limit, the composition dependences of thermoelectric powers are understood in terms of the Heikes formula in a strongly correlated region with the carrier numbers of $2(5-\alpha)$ per coupled V–O–V orbital. This work indicates that in the vicinity of one-dimensional Mott insulator, the effects of atomic disorder and electron correlation for the transport properties may be related to each other.

References

[1] Bouloux J C and Galy J 1973 *Acta Crystallogr.* B **29** 1335
[2] Bouloux J C and Galy J 1973 *Acta Crystallogr.* B **29** 269
[3] Onoda M and Nishiguchi N 1996 *J. Solid State Chem.* **127** 359
[4] Fukumoto Y and Oguchi A 1998 *J. Phys. Soc. Japan* **67** 2205 and references therein
[5] Nishiguchi N, Onoda M and Kubo K 2002 *J. Phys.: Condens. Matter* **14** 5731 and references therein
[6] Onoda M and Hasegawa J 2006 *J. Phys.: Condens. Matter* **18** 2109
[7] Smolinski H, Gros C, Weber W, Peuchert U, Roth G, Weiden M and Geibel C 1998 *Phys. Rev. Lett.* **80** 5164
[8] Onoda M and Kagami T 1999 *J. Phys.: Condens. Matter* **11** 3475
[9] Horsch P and Mack F 1998 *Eur. Phys. J.* B **5** 367
[10] Isobe M and Ueda Y 1996 *J. Phys. Soc. Japan* **65** 1178
[11] See, for a review Lemmens P, Güntherodt G and Gros C 2003 *Phys. Rep.* **375** 1
[12] Onoda M, Ohta H and Nagasawa H 1991 *Solid State Commun.* **79** 281

[13] Shannon R D 1976 *Acta Crystallogr.* A **32** 751
[14] Ogawa K, Onoda M and Nagasawa H 1986 *J. Phys. Soc. Japan* **55** 2129
[15] Ivanov V A, Popovic Z V, Khuong O P and Moshchalkov V V 2001 *Europhys. Lett.* **56** 74
[16] Efros A L and Shklovskii B I 1975 *J. Phys. C: Solid State Phys.* **8** L49
[17] Nguyen V L 1995 *Phys. Lett.* A **207** 379
[18] Burns M J and Chaikin P M 1985 *J. Phys. C: Solid State Phys.* **18** L743
[19] Mott N F 1968 *J. Non-Cryst. Solids* **1** 1
[20] Onoda M 2004 *J. Phys.: Condens. Matter* **16** 8957
[21] Nakhmedov E P, Prigodin V N and Samukhin A N 1989 *Sov. Phys.—Solid State* **31** 368
[22] Brenig W, Döhler G H and Heyszenau H 1973 *Phil. Mag.* **27** 1093
[23] Serota R A, Kalia R K and Lee P A 1986 *Phys. Rev.* B **33** 8441
[24] Sekine Y, Takeshita N, Môri N, Isobe M, Ueda Y, Kosaka M and Uwatoko Y 2001 *J. Phys. Soc. Japan* **70** 3660
[25] Kurkijarvi J 1973 *Phys. Rev.* B **8** 922
[26] Onoda M and Yasumoto M 1997 *J. Phys.: Condens. Matter* **9** 5623
[27] Onoda M and Kohno M 1998 *J. Phys.: Condens. Matter* **10** 1003
[28] Wilson A H 1953 *The Theory of Metals* 2nd edn (Cambridge: Cambridge University Press)
[29] Brenig W, Döhler G H and Wölfle P 1973 *Z. Phys.* **258** 381
[30] Chaikin P M and Beni G 1976 *Phys. Rev.* B **13** 647
[31] Zemljič M M and Prelovšek P 2005 *Phys. Rev.* B **71** 085110
[32] Beni G and Coll C F 1975 *Phys. Rev.* B **11** 573